Technical Design Report for SUAS 2025

UMBC AIAA SUAS

University of Maryland, Baltimore County

aiaa@umbc.edu

Abstract—This paper concisely describes the competition, design, and testing strategy of Gita XI 12, a fixed-wing autonomous unmanned aerial vehicle (UAV) built with the primary task of high performance at the 2025 Student Unmanned Aerial Systems (SUAS) competition. Sensitivity studies were performed while considering team expertise and knowledge for the competition flight strategy and the aircraft build. The aircraft consists of an 8-foot high wing made from XPS foam insulation board laminated with epoxy, S-glass fibreglass, carbon fiber, and Kevlar. Composite carbon fiber pieces attach a twin tractor propulsion system on the leading edge of the wing. Comparatively, the 5.4 ft rectangular fuselage is composed of Readi-Board foam boards and contains our dropping mechanism, payload, electronic systems, and 8.2 feet of carbon fiber tubes telescoped within one another. This central tube provides structure to the plane and serves as the attachment point for core components like the wing, conventional wood tail, and carbon fiber tricycle landing gear mechanism. Several tests were performed to ensure aircraft strength and electronic component reliability, and preflight checks are performed before every takeoff for safety and reliability.

I. COMPETITION STRATEGY

SUAS 2025 is the team's very first SUAS competition in which the team is expected to fly. Being in an institution with no aerospace or robotics department, the team's primary vision is to foster learning and enthusiasm for autonomous aviation. The team's objective is to score at least 60% in the
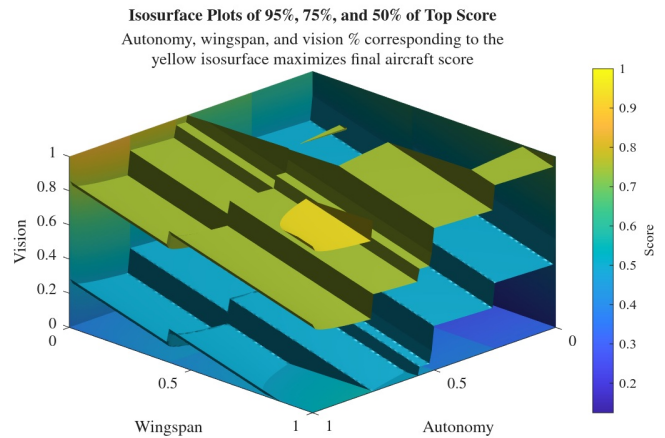

Fig. 1: Mathematical effect of increasing aircraft autonomy, map quality, and wingspan. Higher autonomy, map quality, and larger wingspan yield a better score.

competition with the team's limited knowledge, expertise, and member count of 16.

A sensitivity analysis was performed to determine the mission parameters that best maximize the score for the minimum effort. Figure 1 showcases a 3D sensitivity analysis which was produced by implementing the scoring equations provided in the rules, and scaling variables from 0% to 100% to determine
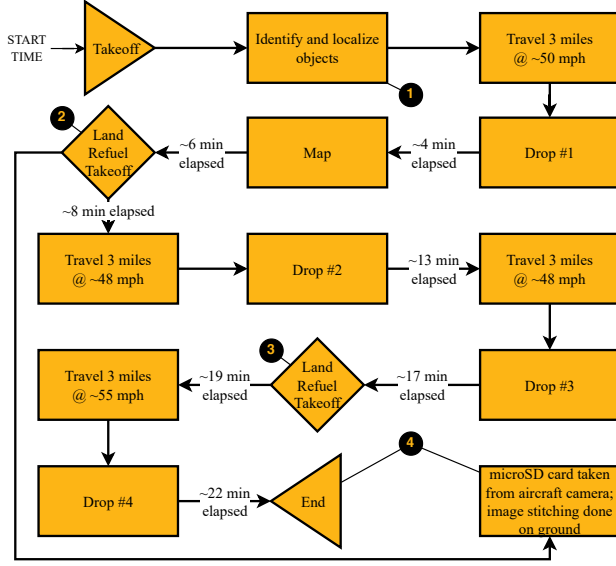
Fig. 2: Actions performed during flight demonstration at competition.

the effect on the score due to tasks involving autonomy, map quality, and wingspan. Increasing the map quality is directly proportional to the final score. Improving the autonomous functions of the aircraft only improves the score up to the point where the discrete requirements are met. Aircraft volume, weight, and the number of operators needed were combined into a single parameter 'wingspan'. The equation for the score s_w due to wingspan $w \in [0, 1]$ is:

$$s_w = \underbrace{\frac{200\lfloor 6w \rfloor}{6}}_{\text{\# of operators}} + \underbrace{50\sqrt[3]{1-w}}_{\text{weight}} + \underbrace{v(w)}_{\text{volume}} \quad (1)$$

where $v(w)$ is the scoring function due to minimizing volume, i.e., the wingspan. The stepwise nature of Figure 1 stems from discrete scoring present in the equation for number of operators and the equation for fitting the plane in a specific volume. In general, a larger wingspan (and therefore a larger plane) is ideal due to less operators required; the exact size of the wing and other design metrics are described in Section II.

In addition to the sensitivity analysis, prior experiences with crashes led the team to prioritize a strong, reliable, and easy to repair aircraft that can be produced with minimum effort and time. The sensitivity analysis determined the overall airplane size and objectives of the competition, while the team values in reliability and simplicity shaped the methodology of constructing the aircraft (described in Section II) and the means of completing the missions at competition.

Figure 2 illustrates the flight strategy at competition. Flight begins with the aircraft carrying a single payload and flying over the objects to identify and localize the items, as indicated by (1) in the diagram. Once localized, a waypoint over one of the object is added. After completing a lap, a third operator is used to manually drop a beacon at the waypoint. As the aircraft

proceeds to map the territory, the third operator prepares for refueling. During refueling, indicated by (2) in the diagram, batteries are swapped, two payload are added, and the mapping camera's microSD card is taken out. As the safety pilot initiates autonomous takeoff, the third operator proceeds to use a secondary computer for stitching the images to a map. While the stitching processes, the third operator continues to drop payloads. During the second refueling (3), only a single payload is attached and dropped. The airplane is designed to be able to travel more than two laps and finish well before the thirty minute limit. The map stitching generally takes 15 minutes; after the final landing (4), the stitched map is taken to the judge and the aircraft is taken off the runway.

II. DESIGN STRATEGY

The design approach for our aircraft prioritized low weight, high strength, and ease of construction and assembly. To achieve this, foam and carbon fiber were selected as the primary construction materials. The aircraft was built around a central carbon fiber boom, allowing for the attachment of multiple components including the foam fuselage, wing, landing gear braces, and tail. This design method transfers the majority of the loads to a strong and rigid structure, preventing failure during adverse conditions such as hard landings.

A. Wing

The wings of Gita XI 12 were first designed using Fermi estimates. The payload weight and the general payload-to-aircraft weight ratio were used to estimate the final aircraft weight to be approximately 20 lb. The aircraft cruise speed was selected to be 48 mph to travel four laps in 15 minutes. The aircraft stall speed was selected to be 25 mph based off of the pilot's comfortable landing speed. The weight, air density, takeoff coefficient of lift, cruise speed, and stall speed were utilized to determine the wing size A and coefficient of lift at cruising C_L (i.e., at $0°$ angle of attack) using the following systems of equation:

$$\underbrace{L}_{\text{weight}} = \frac{1}{2}\underbrace{C_L}_{\text{takeoff}} \times \rho \times A \times \underbrace{v^2}_{\text{cruise}} \quad (2)$$

$$\underbrace{L}_{\text{weight}} = \frac{1}{2}\underbrace{C_L}_{\text{cruise}} \times \rho \times A \times \underbrace{v^2}_{\text{stall}} \quad (3)$$

The wing area was calculated to be $10.6\,\text{ft}^2$, which corresponds to a 8 ft by 1.3 ft wing and a standard aspect ratio of 6 [1]. Several 3D airfoil shapes were iterated on XFLR5 to select the NACA4415 to be the final airfoil. This ensures level flight and low drag at cruising speeds, and the high-wing design ensures enhanced inherent stability [2].

The wing was built from a CNC-cut XPS pink foam core for accurate shaping of the airfoil, and a multi-material composite covering. The composite layup consisted of 2 layers of S-glass covering the full length of the wing for general stiffness and surface durability, 1 layer of carbon fiber plain weave covering the sides of the wing, and 3 layers of carbon fiber plain weave covering the center of the wing where the maximum moment
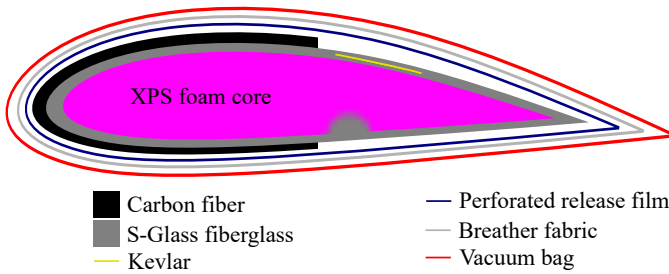
Fig. 3: Wing structure and vacuum bagging layers. Note that the divet in the foam core is for routing wires.

is experienced. Additionally, strips of Kevlar were placed over the hinge points of the flaps and ailerons for local strength. Vacuum bagging was utilized for this wet layup, and the layup structure is illustrated in Figure 3. This composite layup over a foam core provided the optimal tradeoff between strength and weight, though it entailed a high labor build process.

B. Fuselage

The design and fabrication of the Gita XI 12 fuselage involved a repetitive cycle of prototyping and refinement. Foamboard was selected as the primary construction material due to its low weight, affordability, and forgiving nature during testing and modification. Initial prototypes featured a smooth, curved fuselage under the assumption that enhanced aerodynamics would improve performance. However, after an early crash, the team reevaluated this approach and adopted a box-shaped fuselage. When computations were performed in SOLIDWORKS, the rectangular fuselage exhibited a drag of 0.562 lbf, whereas the rounded fuselage showed a drag of 0.225 lbf. The absolute difference between these values is minimal and does not significantly affect our design considerations. The new geometry provides comparable aerodynamic performance while significantly improving manufacturability, repairability, and internal component integration.

The construction process began with the fabrication of internal fuselage ribs. These structural elements established the core framework of the aircraft, setting key component locations such as the wing mount, electronics bay, and empennage attachment. The outer foam shell was then designed to conform to the profile defined by the ribs, resulting in a custom-fit fuselage that maintained structural alignment while minimizing weight.

Fuselage length and configuration were determined based on aircraft balance and stability requirements. A simplified empirical method was employed, wherein the distance from the wing to the tail was measured and multiplied by a factor of two-thirds to define the optimal forward fuselage length. This ratio ensured adequate moment balance between the fore and aft sections of the airframe, contributing to stable flight dynamics.

C. Landing Gear

The landing gear was chosen to be a tricycle configuration in order to provide the best balance and optimize the angle of attack for loaded takeoffs. For this reason, the rear landing
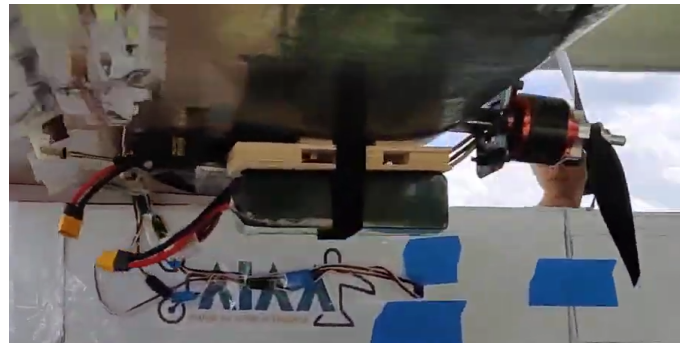

Fig. 4: Propulsion mounting system

gear needed to be designed to handle roughly 85-90% of the total weight of the aircraft and the majority of the landing impact [3]. The rear landing gear was fabricated by laying up 32 layers of carbon fiber plain weave in a custom 3D-printed mold. Though compromising on weight due to its high layer count, this approach ensured the impact strength needed for repeated takeoffs and landings.The front landing gear was designed to handle roughly 10-15% of the total weight of the aircraft as well as a portion of the landing impact [3]. For this purpose, a 4 mm steel rod was chosen as it offers simple construction, low weight, and a high ease of field assembly. For the mounting support of this steel rod inside the fuselage, 2 spaced out steel pieces were chosen to prevent the steel rod from wearing a hole over time into a softer material such as aluminum or plastic.

Both the front and rear landing gear were connected to fuselage-shaped carbon fiber braces. These braces transfer landing loads directly to the main carbon fiber boom, reducing stress on the foam fuselage.

D. Empennage

A conventional tail was selected for structural integrity, reliability, and manufacturability. In the initial Gita XI 12 flights, a V-tail was constructed out of carbon fiber rod reinforced foam board. However, due to lack of structural integrity which led to a crash, the design was switched to a wooden conventional tail covered with Ultracote. Two lightweight servos control the elevator individually; two servos were selected for redundancy and safety. A rudder is present and is controlled using a pull-pull string mechanism, with the servo located on the boom closer to the center of the aircraft. If the rudder were to fail, differential steering would provide additional redundancy.

E. Propulsion System

A propulsion system was selected based on ease of implementation, structural characteristics, and demanded flight time and speed. A twin tractor motor was selected due to the ability to mount batteries underneath the wing, additional thrust, ground and aerial steering using differential thrust, simplicity in wiring, lower prop wash over tail surfaces, and smaller landing gears (since smaller propellers can be used and mounted higher on the wing). Figure 4 showcases the mounting mechanism of the propulsion system onto the wing.
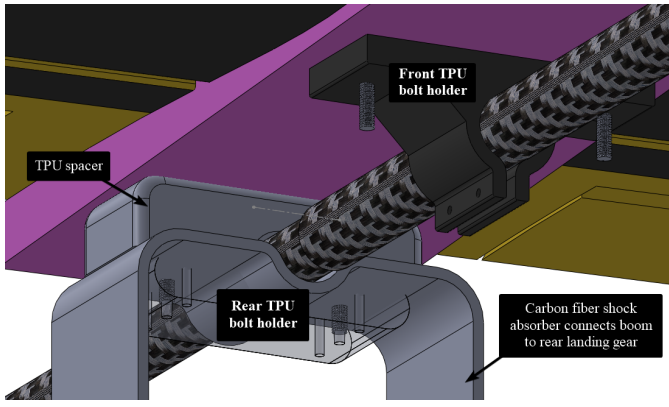
Fig. 5: Wing-Boom Adapters

3D printed molds were to produce seven layer carbon fiber motor mounts that fit flush with the wing. The mounts are bolted together through the wing. A nut with threadlocker was installed at the bottom of the wooden battery holder to secure the motor mount and battery holder in place. Battery straps run through the holder and velcro straps are attached to the under surface of the holder. These two combined secures the battery in all directions, while simultaneously easing the installation by having the components exposed to the outside. This has the added benefit of airflow and cooling. The speed controller is fastened with hoop and loop tape to the underside of the wing next to the battery and motor for airflow and reduced wiring. Servo wire extensions extend the speed controller wiring into the fuselage where the thrust signal is plugged into the flight controller. The exact motor, propeller, and speed controller is specified in Section III.

F. Wing-Boom Adapters

The most secure and reliable means of attaching the composite wing to the central boom was determined to be utilizing four M6 bolts. Holes were drilled into the wing and a pink foam holder (which serves the function of maintain a 0 degree angle of incidence). 3D printed TPU adapters were installed and attached to the boom, as shown in Figure 5. The bolts would go through the wing, the pink foam spacer, and the TPU adapter. The TPU adapters had 4 mm holes for 6mm bolts. This enables the adapters to act as vibration dampening nuts. A TPU spacer is added for the rear bolts. This spacer separates the pink foam from the carbon fiber shock absorber which additionally secures the rear landing gear. This synergestic system ensures ease of assembly through only four bolts, while simultaneously ensuring reliability.

G. Flight Controller

Our aircraft design necessitated a flight controller system with adequate peripheral connections and features while also remaining cost-efficient. Specifically, the absolute requirements for flight-controller features included sufficient UART and PWM signal connections. Additionally, various functional requirements included on-board voltage regulators as both a self power source and PWM power source, as well as analog sensing and sensor redundancy. Compared to numerous available options, the MatekSys H743-WLITE flight controller was selected for meeting the vast majority of both absolute and functional requirements while also remaining significantly less expensive than other popular options such as the Holybro Pixhawk 6C and Holybro Durandal, which was 90% more expensive than the MatekSys model and lacked key features.

H. Radio System

The communication system used on the aircraft was chosen by keeping a focus on reliability, simplicity and redundancy. To meet these requirements, the Mavlink Long Range Signal (mLRS) radio system was chosen for the ground control station alongside ExpressLRS for the pilot controls. The transceivers work on 915 MHz [4] for mLRS, and 2.4 GHz for ELRS. This frequency provides long range transmission (10 km to 100 km) and penetrates obstacles such as trees and the fuselage. The bi-directional nature of the mLRS system allows communication of flight data (telemetry) through the hardware, reducing the complexity of the equipment used on board. The ELRS system focuses on manual takeover and control, and always has higher priority.

The mLRS radio system uses the MAVLink communication protocol which is a very lightweight messaging protocol, developed specifically for unmanned aerial vehicles [4]. The Mavlink protocol is beneficial over other communication protocols such as ELRS or FrSky due to its structured message handling, heartbeat signal health monitor, seamless integration with Mission Planner and most importantly, full-duplex communication. This allows the safety pilot to receive data such as air speed, altitude, pitch, distance from home, etc.

The mLRS receiver module was positioned at a significant distance from the flight controller's power source to minimize electrical noise and signal interference. Since the operating frequency (915 MHz) is relatively low, it offers improved range compared to higher-frequency systems at a cost of lower penetration; consequently, the mLRS antenna was placed outside of the fuselage.

The ELRS receiver module has a 100 mW maximum telemetry power. Due to its higher frequency (2.4 GHz) and lower power, this module was placed inside the fuselage for better aerodynamic performance. The ELRS, mLRS, and video transmitter were all spaced away from each other to minimize interference.

The mLRS transmitter module is capable of connecting to the co-pilot's GCS software. This reduced field setup time and improved the safety pilot's mobility and ease of navigation. Additionally, the use of two separate radio systems significantly improve redundancy and safety. In one of the initial flights where only mLRS was used for both ground control station and manual control, the receiver lost signal leading to a crash during RTL. After solving the signal loss issue, the team chose to utilize a redundant ELRS system for manual control to ensure that, in the event that either radio system loses connection, control will be maintained at all times through either the GCS or pilot controls if not both.

I. Flight Sensors

Three primary sensors — ground facing LiDAR, GPS (with compass), and airspeed — were chosen to provide adequate in-flight telemetry data for both manual and autonomous flight. LiDAR was used to serve as a more accurate instrument for altitude measurement compared to barometers, where error is often present due to changes in pressure throughout different environments and the suboptimal conditions of being mounted to an aircraft. Further, GPS was required to track the physical location of the aircraft in flight — a critical instrument to enable waypoint missions and record necessary data such as distance from home and total distance traveled. Lastly, an airspeed sensor was essential for gathering accurate values for speeds of the aircraft relative to its position in surrounding air, as ground speed sensing fails to account for traveling through wind and lift produced by wings. By tracking relative airspeed, critical details such as stall speed and cruising speed can be accurately calculated.

J. Dropping Mechanism

With the competition aircraft being a fixed wing plane, the dropping mechanism needs to not have significant aerodynamic drag in order to increase flight time. Using an enclosed self-closing bay within the fuselage, harnessing the venturi effect, to mitigate pressure drag after deployment increases flight time therefore minimizing refueling during competition. Within this enclosed system exists an actuated pin, controlled by a servo using rotary-to-linear conversion linkage, in which the payload is attached to. Once the servo is activated, the pin actuates backwards which detaches the LED beacon from the aircraft causing gravity to pull the projectile out of the bay. Since the payload is propping the bay open, once it leaves the plane, the high speed and low pressure air sucks the bay closed.

A third operator will be used for the payload drop. Using another operator equipped with a FPV headset and a radio controlled switch, the payload is dropped based on the predicted freefall location. Using an automatic stabilised deploying drogue shoot like appendages, the targeted location is easier to hit due to the predictability of the high drag shoot while slowing down the LED beacon from breaking on impact. During the competition, first the plane scans the predicted target location, then on a different pass, the aircraft flies directly over the target and the operator drops the payload according to the predicted flight path of the projectile. During a refuelling, the payload operator loads the aircraft by triggering the servo to actuate forward once the pin is inline with the fastener within each payload. This simple and reliable mechanism enables fast, repeatable payload loading, maximizing mission performance.

K. Avoidance

Two long-range ESP32 will be utilized to detect Bluetooth and WiFi RemoteID (RID) broadcasts as a part of the collision detection system (CDS). The 3D position vector $\mathbf{x}$ and computed velocity vector $\dot{\mathbf{x}}$ from the RID broadcasts are utilized to determine whether two aircrafts are likely to collide. The equation

$$||(\dot{\mathbf{x}}_a t + \mathbf{x}_a) - (\dot{\mathbf{x}}_b t + \mathbf{x}_b)|| \leq R_{\text{UAV collision}} \qquad (4)$$

calculates whether two aircraft are within a certain $R_{\text{UAV collision}}$ distance from each other at time t. The time where the aircrafts are in closest proximity to each other, t_{col}, is given by

$$t_{\text{col}} = \frac{-\dot{\mathbf{x}}_1^\top \mathbf{x}_1 + \dot{\mathbf{x}}_1^\top \mathbf{x}_2 + \dot{\mathbf{x}}_2^\top \mathbf{x}_1 - \dot{\mathbf{x}}_2^\top \mathbf{x}_2}{\dot{\mathbf{x}}_1^\top \dot{\mathbf{x}}_1 - 2\dot{\mathbf{x}}_1^\top \dot{\mathbf{x}}_2 + \dot{\mathbf{x}}_2^\top \dot{\mathbf{x}}_2}. \qquad (5)$$

These two equations will be implemented on the CDS. The CDS will produce audible sounds and visual lighting to alert the safety pilot and GCS operator of a potential collision between Gita XI 12 and foreign aircrafts, and therefore switch to loiter or guided mode to avoid a collision. Although the team made software for the aircraft to fully autonomously avoid foreign aircrafts, the increased level of complexity and hardware introduced additional safety and reliability concerns. This simplified CDS aids the safety pilot in taking timely avoidance maneuvers since the CDS is not susceptible to lack of visibility and depth perception.

III. TESTING STRATEGY

A. Flight safety checklist

Prior to every operational instance, a comprehensive safety inspection is conducted to confirm that the Gita XI 12 aircraft is in proper working order. This inspection follows a standardized checklist to prevent minor anomalies from escalating into significant issues during flight operations. The procedure encompasses all major systems of the aircraft, ensuring it is fully prepared for flight.

The inspection commences with an evaluation of the control surfaces. The ailerons, elevator, flaps, and rudder are manually cycled through their full range of motion to verify smooth operation. Subsequently, the propulsion system undergoes rigorous testing. The motor is started and operated through varying throttle settings to assess response characteristics.

A detailed examination of the avionics systems is performed. The battery charge level is verified, and the functionality of GPS, telemetry, and other electronic systems is confirmed. Any weak signal strength or system failure necessitates thorough troubleshooting prior to continuing the inspection process.

Finally, a thorough visual structural inspection is executed. The integrity of the landing gear, fuselage, and wing-to-boom adapter is assessed for any signs of damage, stress, or misalignment. All components must be securely fastened and properly aligned.

Once structural integrity has been verified, the center of gravity (CG) is evaluated. For the Gita XI 12, the target CG location is approximately 25% of the mean aerodynamic chord (MAC). Achieving the correct balance is critical to ensuring stable and predictable flight behavior. After confirming CG alignment, a brief thrust test is conducted to verify that the aircraft can attain the required takeoff speed.

While these steps are consistently performed prior to every operational instance, they are not treated as routine procedures. Each inspection provides an opportunity to identify potential issues early and mitigate risks associated with flight operations. Adhering to this structured process is essential for maintaining aircraft integrity and ensuring safe operation under all conditions.

B. Composite Parts Testing

All composite parts were tested for safety and durability. All surfaces were inspected to ensure that no sharp frays were exposed; where necessary, frays were sanded or taped over. A wing tip test was performed where the wing was lifted on the tips, and a 25 lb payload was placed at the center: this simulates a 2.5g wing loading. The wing deflected at the center only by 0.25 in. Next, individuals weighing between 55 lb and 100 lb were asked to sit on the middle of the wing. Although there were some deflections, the wing did not fail. The carbon fiber motor mounts were tested by applying 25 lb of force in the direction of thrust; all mounts passed. The carbon fiber rear landing gear was tested by applying 140 lb at the center; the landing gear deflected by no more than 0.5 in. The composite shock absorbers were similarly tested.

C. Flight Sensor & Radio Tests

Non-propulsion electronics are tested after any modifications made; all flight-related sensors are tested before flight. The ELRS and mLRS radio systems are checked to ensure they: successfully transfer data, do not lose telemetry packets, are adequately cooled, and have adequate power supply to survive flights. Before every flight, the team ensures that the GPS has a 3D fix, barometer and LiDAR have an accurate reading of the distance from ground, airspeed sensor provides a reading when air is blown on it, compass provides accurate heading even when propulsion system is running, and the flight controller has correct acceleration and gyroscopic readings. To ensure a successful pass, the aircraft is held steady, the pitot tube is covered, and the aircraft is on the ground outside during boot: this correctly calibrates the accelerometer and gyroscope of the flight controller and calibrates the zero point of the airspeed sensor, and allows a GPS fix [5].

D. Propulsion Testing

Motors and their corresponding manufacturer recommended propeller were tested with 6S LiPo 4500 mAh batteries (which are just under the 100 Wh limit) on a dynamic thrust test stand (DTTS). The DTTS was mounted on a car driving at the cruise speed of the aircraft. The motor was run from 0% to 100% throttle. The DTTS records the force, current, and voltage. These measurements were used to determine the power draw and the flight time on the selected battery. For an expected aircraft drag of 5 N, the expected cruise flight time is 15.6 minutes. This result roughly corresponds to the flight results. A 10 minute flight at cruising speeds depleted the battery from 96% to 40%. The team finalized two Spektrum Avian 5055 650 KV motors with 12x6 or 12x8 (depending on flight speed) propellers as the propulsion of choice.

E. Testing Autonomy

The team built a twin-motor conventional tail tricycle landing gear aircraft out of foamboard to replicate control surface and flight characteristics of the Gita XI 12. This aircraft was used to test all aspects of autonomous flights: PID tuning, TECS tuning, navigation tuning, testing autonomous takeoff/flight/landing, and more. Utilizing a 2 lb test aircraft to gain practice with autonomy and its setup significantly aided the team in gaining experience with autonomous systems and ensuring the safety of the Gita XI 12. Afterwards, tests were performed on the competition aircraft: autotune was performed to better synchronize stick movement with aircraft attitude, navigation tuning was performed to ensure that aircraft can pass through waypoints correctly, TECS tuning was performed to improve ascend and descend rates, and more. Each new autonomous mission is tested on Mission Planner's simulation page; next, these are tried on the test aircraft before risking Gita XI 12.

REFERENCES

[1] S. Shaha, M. Sadiq, and A. Pachapuri, *Naca 2415-finding lift coefficient using cfd, theoretical and javafoil*, IJRET: International Journal of Research in Engineering and Technology. [Online]. Available: https://ijret.org/volumes/2015v04/i07/IJRET20150407070.pdf.

[2] P. Institute, *Low wing vs. high wing aircraft: Pilotinstitute*, Pilot Institute, Nov. 2022. [Online]. Available: https://pilotinstitute.com/high-wing-vs-low-wing/.

[3] D. Raymer, *Aircraft design: a conceptual approach*. American Institute of Aeronautics and Astronautics, Inc., 2012.

[4] *Mlrs mavlink 900mhz receiver, mr900-30 – matek systems*, Mateksys.com, 2025. [Online]. Available: https://www.mateksys.com/?portfolio=mr900-30 (visited on 05/09/2025).

[5] *Starting up and calibrating plane — plane documentation*, Ardupilot.org, 2024. [Online]. Available: https://ardupilot.org/plane/docs/starting-up-and-calibrating-arduplane.html (visited on 05/12/2025).